applied microbiology

MDPI

Article

Revisiting the LuxS/AI-2–SdiA Regulatory Network in *Klebsiella pneumoniae*: Context-Dependent Modulation by Halogenated Thiolactones

Sinethemba H. Yakobi * and Uchechukwu U. Nwodo

Patho-Biocatalysis Group (PBG), Department of Biotechnology and Biological Sciences, University of Fort Hare, Private Bag X1314, Alice 5700, South Africa
* Correspondence: syakobi@ufh.ac.za

Abstract

Quorum sensing (QS) represents a promising target for anti-virulence therapy; however, effective pharmacological intervention requires a detailed understanding of regulatory network architecture and environmental context. In *Klebsiella pneumoniae*, the orphan LuxR-type receptor SdiA lacks a cognate LuxI synthase and instead detects exogenous acyl-homoserine lactones (AHLs), positioning it as an inter-species signal integrator. Here, we demonstrate that SdiA functions as a context-dependent regulator whose impact on biofilm formation and virulence gene expression is gated by environmental AHL availability. Using isogenic ΔluxS, ΔsdiA, and ΔluxSΔsdiA mutants in a clinical bloodstream isolate, we show that under AHL-limited conditions, SdiA promotes baseline biofilm development, whereas in the presence of exogenous C6-HSL, it restrains excessive biofilm maturation. Two-way ANOVA confirmed significant genotype, treatment, and interaction effects, establishing that SdiA-mediated regulation is signal contingent. We further investigated the halogenated thiolactone meta-bromo-thiolactone (mBTL), previously described as a QS inhibitor in *Pseudomonas aeruginosa*. In *K. pneumoniae*, mBTL acts as a context-selective modulator rather than a simple inhibitor. Under AHL-limited conditions, mBTL phenocopied ΔsdiA, reducing biofilm formation and inducing overlapping transcriptional profiles. In contrast, under AHL-replete conditions, mBTL opposed SdiA-dependent gene expression, consistent with competitive antagonism of ligand-bound receptor. RNA-seq analysis revealed substantial concordance between ΔsdiA and WT + mBTL under AHL-free conditions, with the inversion of transcriptional directionality in the presence of C6-HSL. The findings redefine SdiA as a conditional quorum-sensing integrator and identify mBTL as a ligand-context-dependent modulator of LuxR-type signaling. Our results highlight the necessity of evaluating anti-virulence compounds across relevant signal environments and introduce receptor state-selective modulation as a strategic framework for targeting hybrid quorum-sensing systems in polymicrobial pathogens.

Keywords: *Klebsiella pneumoniae*; quorum sensing; SdiA; LuxS; mBTL; biofilm; anti-virulence

Check for updates

Academic Editor: Filomena Nazzaro

Received: 18 October 2025
Revised: 23 February 2026
Accepted: 26 February 2026
Published: 27 March 2026

Copyright: © 2026 by the authors. Licensee MDPI, Basel, Switzerland. This article is an open access article distributed under the terms and conditions of the Creative Commons Attribution (CC BY) license.

1. Introduction

The global dissemination of multidrug-resistant *Klebsiella pneumoniae* (*K. pneumoniae*)—particularly hypervirulent (hvKP) and carbapenem-resistant (CRKP) lineages—has created an urgent need for therapeutic strategies that circumvent conventional antibiotic resistance mechanisms [1,2]. Anti-virulence approaches, which aim to disarm pathogens rather than

kill them, offer the theoretical advantage of reducing selective pressure for resistance while preserving host microbiota [3]. Among bacterial traits suitable for such intervention, quorum sensing (QS)—the cell-density-dependent communication system that coordinates collective behaviors—has emerged as a particularly attractive target [4,5]. *K. pneumoniae* possesses an unusual QS architecture that distinguishes it from canonical LuxI/LuxR-type Gram-negative pathogens [6,7]. The organism harbors a functional LuxS/AI-2 system, which synthesizes the interspecies signaling molecule autoinducer-2 (AI-2) and regulates diverse processes including biofilm formation, motility, and recently, plasmid conjugation [8–10]. Simultaneously, *K. pneumoniae* encodes SdiA, an orphan LuxR-type receptor that lacks a cognate LuxI synthase and instead detects exogenous acyl-homoserine lactones (AHLs) produced by neighboring bacterial species [11,12]. This hybrid architecture enables *K. pneumoniae* to detect and integrate quorum-sensing signals produced by neighboring microorganisms into its own regulatory circuitry. The functional role of SdiA in *K. pneumoniae* virulence has been the subject of considerable debate. Early studies suggested that SdiA contributes positively to biofilm development and fimbrial gene expression under certain conditions [13]. However, subsequent investigations revealed that sdiA deletion can enhance biofilm formation, pointing to a repressive function [14]. Both Pacheco et al. and Silva-Bea et al. demonstrated that SdiA suppresses fimbriae expression and biofilm formation in *K. pneumoniae*, with sdiA mutants exhibiting increased biomass and autoinducer production [13,15]. More recently, Silva-Bea et al. reported that sdiA deficiency promotes biofilm maturation and cell filamentation while increasing susceptibility to phage infection, with the regulatory outcome heavily influenced by AHL availability [5,16]. These apparently contradictory findings underscore a fundamental principle: SdiA does not function as a unidirectional virulence switch but rather as a conditional signal integrator whose output depends critically on the presence, identity, and timing of exogenous AHL cues [17,18]. This context-dependency has profound implications for anti-virulence drug development. Small molecules that target SdiA cannot be assumed to produce uniform phenotypic effects across conditions; rather, their activity must be understood in relation to the prevailing signal environment. The halogenated thiolactone meta-bromo-thiolactone (mBTL) exemplifies this complexity. Originally identified as a QS inhibitor in *Pseudomonas aeruginosa* (*P. aeruginosa*) through its partial antagonism of LasR and RhlR [17], mBTL has subsequently been shown to modulate QS phenotypes in diverse bacterial species [19]. However, whether such compounds retain activity in organisms lacking canonical LuxI/R systems—and whether their effects are truly inhibitory or contextually modulatory—remains poorly characterized. In the present study, we systematically investigate the LuxS/AI-2–SdiA signaling axis in *K. pneumoniae* using a combination of genetic dissection, pharmacological profiling, and infection modeling. Our aims were threefold: first, to reconcile conflicting reports regarding SdiA function by systematically varying AHL availability; second, to evaluate whether halogenated thiolactones previously characterized in *P. aeruginosa* retain activity against the *K. pneumoniae* QS network; and third, to determine whether mBTL functions as a simple inhibitor or as a context-dependent modulator whose phenotypic effects are gated by signal availability. By integrating these approaches, we demonstrate that mBTL acts as a selective SdiA modulator whose anti-virulence efficacy depends critically on the genetic background and AHL environment—findings that inform both the mechanistic understanding of QS regulation and the rational development of precision anti-infective strategies.

2. Materials and Methods

2.1. Bacterial Strains and Growth Conditions

K. pneumoniae strain KP-PA45, a bloodstream isolate from a patient with healthcare-associated infection, was used as the wild-type background for all experiments. The strain

was selected for its robust biofilm phenotype and susceptibility to genetic manipulation. Isogenic deletion mutants (ΔluxS, ΔsdiA, and ΔluxSΔsdiA) were constructed using λ-Red recombinering as previously described [20], with gene deletions confirmed by PCR and Sanger sequencing. *Escherichia coli* BL21-Gold (DE3) (Agilent Technologies, Santa Clara, CA, USA) was used for heterologous protein expression and reporter assays. *Vibrio harveyi* BB170 (ATCC BAA-1117; American Type Culture Collection, Manassas, VA, USA) was used for AI-2 bioluminescence assays.

Unless otherwise specified, bacteria were cultured in Luria–Bertani (LB) broth (Sigma-Aldrich, Johannesburg, South Africa) at 37 °C with shaking (200 rpm) in a shaking incubator (New Brunswick™ Innova® 44, Eppendorf, Hamburg, Germany). For biofilm assays, M9 minimal medium (Sigma-Aldrich, Johannesburg, South Africa) supplemented with 0.4% glucose and 0.2% casamino acids (BD Difco™, Becton, Dickinson and Company, Sparks, MD, USA) was used to minimize confounding effects of rich media on QS outputs. Where indicated, cultures were supplemented with N-hexanoyl-L-homoserine lactone (C6-HSL; Sigma-Aldrich, Johannesburg, South Africa) at concentrations ranging from 0.1–10 μM. Antibiotics were used at the following concentrations when required: ampicillin (100 μg/mL), kanamycin (50 μg/mL), and gentamicin (15 μg/mL) (Sigma-Aldrich, Johannesburg, South Africa).

2.2. Compound Synthesis and Preparation

Halogenated thiolactone analogs—chloro-lactone (CL), chloro-thiolactone (CTL), meta-chloro-thiolactone (mCTL), and meta-bromo-thiolactone (mBTL)—were synthesized as previously described. Purity (>95%) was confirmed by high-performance liquid chromatography (HPLC; Agilent 1260 Infinity II, Agilent Technologies, Santa Clara, CA, USA) and nuclear magnetic resonance spectroscopy (Bruker Avance III HD 400 MHz, Bruker Corporation, Billerica, MA, USA). Compounds were dissolved in DMSO (Sigma-Aldrich, Johannesburg, South Africa) to prepare 100 mM stock solutions and stored at −20 °C in single-use aliquots. For all experiments, final DMSO concentrations were $\leq$0.1% (*v*/*v*), and vehicle-only controls were included to control for solvent effects.

2.3. Growth, Viability, and Cytotoxicity Controls

To exclude bacteriostatic, bactericidal, or host-cell toxic effects of mBTL, growth kinetics, viable counts, AI-2 normalization, and compound-only cytotoxicity controls were performed. For growth curves, overnight cultures of *K. pneumoniae* KP-PA45 were diluted to OD_{600} = 0.05 in LB or defined M9 medium containing vehicle (0.1% DMSO) or 100 μM mBTL. OD_{600} was recorded every 15 min for 16 h, and growth rate (μ), lag time, and maximum OD_{600} were estimated by nonlinear regression. For viable counts, cultures grown under 24 h static biofilm conditions (±mBTL; ±C6-HSL) were serially diluted and plated for CFU enumeration. AI-2 reporter output was normalized to culture density at the time of supernatant collection (RLU/OD_{600}). For host-cell controls, uninfected A549 monolayers were exposed to 100 μM mBTL for 6 h, and LDH release was quantified relative to Triton X-100 lysis controls. The OD_{600} measurements were recorded using a BioTek Synergy H1 microplate reader (BioTek Instruments, Winooski, VT, USA). LDH release was quantified using the CytoTox 96® Non-Radioactive Cytotoxicity Assay (Promega Corporation, Madison, WI, USA) relative to Triton X-100 (Sigma-Aldrich, Johannesburg, South Africa) controls.

2.4. AI-2 Activity Assay

AI-2 accumulation in *K. pneumoniae* culture supernatants was quantified using the *V. harveyi* BB170 bioluminescence reporter assay as described [21]. Overnight *K. pneumoniae* cultures were diluted 1:1000 into fresh LB medium containing test compounds (0.2–200 μM)

or DMSO vehicle and incubated for 16 h at 37 °C with shaking. Cultures were centrifuged (16,000× *g*, 10 min, 4 °C) (Eppendorf 5424 R, Eppendorf, Hamburg, Germany), and supernatants were filter-sterilized (0.22 µm) (MilliporeSigma, Burlington, MA, USA). *V. harveyi* BB170 was grown in AB medium at 30 °C to an OD_{600} of 0.2, then diluted 1:5000 in fresh AB medium. Cell-free supernatants (10 µL) were mixed with 90 µL of diluted reporter culture in 96-well white microplates. Luminescence was measured every 30 min for 6 h using a BioTek Synergy H1 microplate reader (BioTek Instruments, Winooski, VT, USA) [22]. AI-2 activity was calculated as relative luminescence units (RLU) normalized to DMSO controls. Dose–response curves were fitted using nonlinear regression (JMP Clinical version 18; SAS Institute Inc., Cary, NC, USA) to determine IC_{50} values. [23].

2.5. SdiA Reporter Assays

A heterologous *E. coli* reporter system was constructed to assess SdiA modulatory activity. The *K. pneumoniae* sdiA coding sequence was amplified from KP-PA45 genomic DNA and cloned into pET23b (Novagen, Madison, WI, USA) to generate pET23b-sdiA. A transcriptional fusion of the fimA promoter (amplified from KP-PA45) to gfp was constructed in pPROBE-gfp[TT] [24] to generate pfimA–gfp. *E. coli* BL21-Gold (DE3) was co-transformed with pET23b-sdiA and pfimA–gfp.

For agonism assays, overnight cultures were diluted 1:100 into fresh LB containing test compounds (1–200 µM) or DMSO and incubated at 37 °C with shaking. GFP fluorescence (excitation 485 nm, emission 528 nm) and OD_{600} were measured hourly for 8 h using a microplate reader. For antagonism assays, cultures were co-treated with test compounds and C6-HSL at its EC_{95} concentration (determined from preliminary dose–response experiments). Fluorescence values were normalized to cell density (RFU/OD_{600}) and expressed as percentage of maximal C6-HSL-induced fluorescence.

2.6. Biofilm Formation Assays

Static biofilm formation was assessed in 96-well glass-bottom plates (Greiner Bio-One GmbH, Kremsmünster, Austria) as described. Overnight cultures were diluted to OD_{600} = 0.05 in M9 minimal medium and 200 µL aliquots were dispensed per well. Where indicated, compounds (100 µM) and/or C6-HSL (1 µM) were added. Plates were incubated statically at 37 °C for 24 h. For crystal violet (Sigma-Aldrich, Johannesburg, South Africa) quantification, wells were washed twice with phosphate-buffered saline (PBS), air-dried, stained with 0.1% crystal violet for 15 min, washed three times with distilled water, and destained with 30% acetic acid. Absorbance was measured at 595 nm [8].

For confocal microscopy, biofilms were grown in 8-well chambered coverglass slides (Ibidi GmbH, Gräfelfing, Germany). After 24 h incubation, biofilms were gently washed with PBS and stained with 5 µM SYTO9 (Invitrogen™, Thermo Fisher Scientific, Waltham, MA, USA) for 20 min in the dark. Images were acquired using a Zeiss LSM 880 confocal microscope with a 40×/1.2 NA water immersion objective (Carl Zeiss AG, Oberkochen, Germany). Z-stacks were acquired with 0.5 µm intervals and biofilm parameters (biomass, thickness, roughness) were quantified using COMSTAT2 [25]. At least five fields per condition from three independent experiments were analyzed.

2.7. RNA Extraction and Transcriptomic Analysis

For transcriptomic profiling, WT and ΔsdiA strains were grown in M9 minimal medium to mid-exponential phase (OD_{600} = 0.5) in the presence or absence of 100 µM mBTL, with or without 1 µM C6-HSL. Cultures were harvested by centrifugation (10,000× *g*, 2 min, 4 °C) and immediately frozen in liquid nitrogen. Total RNA was extracted using the RNeasy Mini Kit (Qiagen GmbH, Hilden, Germany) with on-column DNase digestion (RNase-Free

DNase Set, Qiagen GmbH, Hilden, Germany). RNA integrity was verified using an Agilent 2100 Bioanalyzer (RIN $\geq$ 8.5) (Agilent Technologies, Santa Clara, CA, USA).

Library preparation and sequencing were performed by Novogene (Cambridge, UK) using the Illumina NovaSeq 6000 platform (Illumina, San Diego, CA, USA) with 150 bp paired-end reads. Raw reads were quality-filtered and mapped to the *K. pneumoniae* KP-PA45 reference genome using Bowtie2 [26]. Read counts were quantified using featureCounts and differential expression analysis was performed using DESeq2 with an FDR threshold of 0.05 and $|\log_2 FC| \geq 1$ [27]. Principal component analysis was performed on variance-stabilized transformed counts. Heatmaps were generated using the pheatmap package in R.

2.8. Microfluidic Biofilm Clogging Assay

Microfluidic flow cells (sticky-Slide VI 0.4; Ibidi GmbH, Gräfelfing, Germany) were inoculated with mid-log-phase cultures diluted to OD_{600} = 0.05 in M9 medium. After 1 h static adhesion, flow was initiated at 0.5 µL/min using a syringe pump (Harvard Apparatus, Holliston, MA, USA). Channels were monitored by phase-contrast microscopy (10× objective) at 12 h intervals. Time to clogging was defined as the point at which flow ceased due to biofilm obstruction, determined by cessation of bead movement (1 µm fluorescent beads(Thermo Fisher Scientific, Waltham, MA, USA) added to the medium as flow tracers) [28]. At least eight independent channels were analyzed per condition.

2.9. Galleria mellonella Infection Model

To increase translational relevance and reduce confounding interpretation, we replaced the *C. elegans* fast-kill model with *Galleria mellonella*. *G. mellonella* larvae (250 mg, final instar; Livefood UK Ltd., Sheffield, UK) were used within 24 h of receipt. Larvae were randomly assigned to treatment groups (n = 15 per group) and stored in the dark at 15 °C prior to use. *K. pneumoniae* cultures were grown to mid-exponential phase, washed twice in PBS, and adjusted to 5×10^7 CFU/mL. Bacterial suspensions (10 µL; 5×10^5 CFU) were injected into the last left proleg using a Hamilton syringe (Hamilton Company, Reno, NV, USA). For compound-treated groups, bacteria were pre-incubated with 100 µM mBTL for 30 min prior to injection. For AHL supplementation experiments, bacteria were pre-incubated with 1 µM C6-HSL for 30 min. Control larvae received PBS or compound alone. Larvae were incubated at 37 °C in the dark and survival was monitored every 6 h for 72 h. Larvae were considered dead when unresponsive to gentle prodding [29]. Experiments were repeated three times with independent biological replicates. Survival curves were analyzed using the log-rank (Mantel–Cox) test.

2.10. A549 Cytotoxicity Assay

Human lung epithelial A549 cells (ATCC CCL-185; American Type Culture Collection, Manassas, VA, USA) were cultured in DMEM (Gibco™, Thermo Fisher Scientific, Waltham, MA, USA) supplemented with 10% fetal bovine serum (Gibco™, Thermo Fisher Scientific, Waltham, MA, USA) and 1% penicillin-streptomycin (Gibco™, Thermo Fisher Scientific, Waltham, MA, USA) at 37 °C in 5% CO_2. For infection assays, cells were seeded in 96-well plates at 2×10^4 cells/well and grown to 80% confluence. *K. pneumoniae* cultures were grown to mid-exponential phase, washed, and resuspended in DMEM without antibiotics at 2×10^7 CFU/mL. For compound-treated groups, bacteria were pre-incubated with 100 µM mBTL for 30 min. For AHL supplementation experiments, bacteria were pre-incubated with 1 µM C6-HSL. Cells were infected at MOI = 10 for 6 h [30]. Cytotoxicity was assessed using the CytoTox 96 Non-Radioactive Cytotoxicity Assay (Promega Corporation, Madison, WI, USA), which measures lactate dehydrogenase (LDH) release. Percent cytotoxicity was calculated

as: (experimental release − spontaneous release)/(maximum release − spontaneous release) × 100. Maximum release was determined by lysing uninfected cells with 0.1% Triton X-100.

2.11. Statistical Analysis

All experiments were performed with ≥3 independent biological replicates unless otherwise stated. Technical replicates were averaged prior to statistical testing. Two-way ANOVA was used for genotype × treatment analyses, with genotype, treatment, and interaction terms specified as fixed effects. Where significant effects were detected, Tukey's HSD was applied for post hoc multiple comparisons. Model assumptions were evaluated by residual inspection and Shapiro–Wilk testing; homogeneity of variance was assessed by residual dispersion across fitted values. For pairwise comparisons, two-tailed Student's *t*-tests (parametric) or Mann–Whitney tests (nonparametric) were applied as appropriate. Survival curves were analyzed using the log-rank (Mantel–Cox) test. Differential expression analysis was conducted using DESeq2 with FDR correction (Benjamini–Hochberg). Unless otherwise indicated, significance was defined as $p < 0.05$. Data are presented as mean ± SD. Statistical analyses were performed using JMP Clinical version 18 (SAS Institute Inc., Cary, NC, USA).

3. Results

3.1. Integrated Model of LuxS/AI-2 and SdiA Signaling in Klebsiella pneumoniae

As illustrated in Figure 1, quorum sensing (QS) regulation in *K. pneumoniae* operates through two interconnected yet mechanistically distinct pathways: the LuxS/AI-2 system and the SdiA receptor-mediated circuit. The LuxS enzyme catalyzes synthesis of autoinducer-2 (AI-2), which is subsequently internalized via the Lsr transporter system. The intracellular phosphorylation of AI-2 promotes binding to the LsrR repressor complex, triggering dissociation from promoter regions and derepression of downstream genes. This cascade has been associated with transcriptional activation of loci associated with biofilm maturation, capsule biosynthesis, and virulence factor production. In parallel, the SdiA system functions as an orphan LuxR-type receptor responsive to exogenous acyl-homoserine lactones (AHLs), such as C6-HSL. Ligand binding stabilizes the SdiA protein, facilitating dimerization and high-affinity interaction with lux-box–like promoter elements. Subsequent recruitment of RNA polymerase initiates transcription of QS-regulated targets, including fimbrial (fimA) and biofilm-associated genes. Collectively, these pathways converge on phenotypes central to pathogenic persistence—virulence and biofilm formation—providing a dual regulatory framework for environmental signal integration.

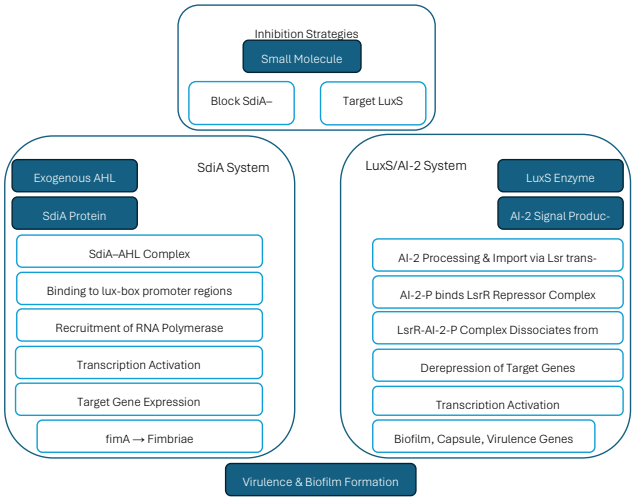


Figure 1. The processes of the LuxS/AI-2 and SdiA quorum sensing systems in *K. pneumoniae*.

3.2. Design and Structural Rationale of Halogenated Thiolactone Analogs

To pharmacologically interrogate this hybrid QS architecture, a focused library of halogenated thiolactone derivatives was developed (Figure 2). The panel comprised chloro-lactone (CL, Figure 2A), chloro-thiolactone (CTL, Figure 2B), meta-chloro-thiolactone (mCTL, Figure 2C), and meta-bromo-thiolactone (mBTL, Figure 2D). These compounds were rationally designed as structural mimetics of canonical homoserine lactones (HSLs), the principal autoinducers in Gram-negative LuxI/LuxR systems.

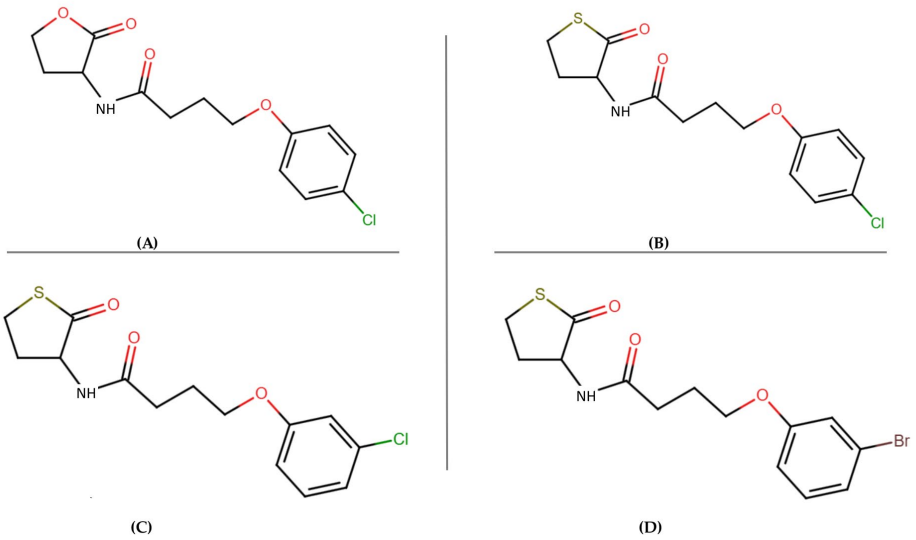


Figure 2. Chemical structures of halogenated thiolactone analogs designed as quorum-sensing inhibitors. The focused library includes chloro-lactone (CL, (**A**)), chloro-thiolactone (CTL, (**B**)), meta-chloro-thiolactone (mCTL, (**C**)), and meta-bromo-thiolactone (mBTL, (**D**)).

Substitution of the lactone oxygen with sulphur (thiolactone scaffold) was introduced to enhance hydrolytic stability and modulate electronic distribution within the ring, potentially improving receptor engagement and resistance to enzymatic degradation. Strategic halogenation at the para- or meta-position of the aromatic moiety was incorporated to increase lipophilicity, promote favorable hydrophobic contacts within LuxR-type binding pockets, and fine-tune steric complementarity. The brominated analog (mBTL) further enabled assessment of size and polarizability effects on receptor interaction dynamics.

Although *K. pneumoniae* lacks a canonical LuxI/R pair, its LuxS/AI-2 and SdiA systems present mechanistic parallels that can be exploited by HSL analogs. The structural homology between SdiA and LuxR-type receptors supports the premise that halogenated thiolactones may competitively interfere with ligand binding or receptor stabilization. In parallel, perturbation of LuxS/AI-2 signaling may arise indirectly through cross-regulatory effects on QS-controlled transcriptional networks.

3.3. Growth and Viability Controls Confirm Non-Bactericidal Activity

To verify that reduced quorum-sensing outputs were not attributable to impaired growth, we quantified planktonic growth kinetics in the presence of 100 μM mBTL. Growth curves in both LB and defined M9 media were indistinguishable from vehicle controls (Figure 3). Estimated growth rate (μ), lag phase, and maximum OD_{600} did not differ significantly between conditions (all $p > 0.05$; Table 1). Similarly, viable counts under 24 h static biofilm conditions were not significantly altered by mBTL treatment ($p > 0.05$), indicating preserved cellular viability.

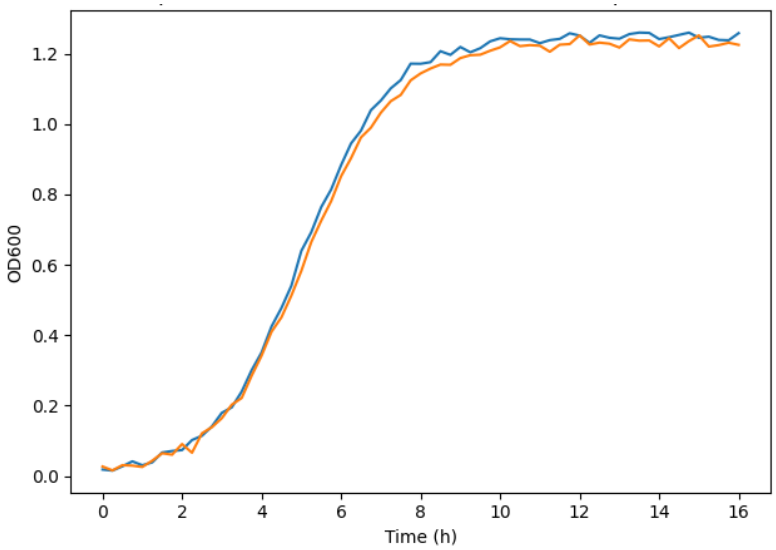


Figure 3. Planktonic growth curves of *K. pneumoniae* KP-PA45 in the presence of vehicle or 100 μM mBTL. OD_{600} was monitored over 16 h in shaking culture. Curves represent mean values of biological replicates. No significant differences in growth rate, lag phase, or maximum density were observed between conditions ($p > 0.05$). Blue indicates the vehicle control (0.1% DMSO); Orange indicates cultures treated with 100 μM mBTL.

Table 1. Growth Parameters of *K. pneumoniae* KP-PA45 ± mBTL.

Condition	Growth Rate (μ, h^{-1})	Lag Phase (h)	Max OD600	Statistical Comparison (*p*-Value)
Vehicle (0.1% DMSO)	0.90	4.8	1.25	0.41
mBTL (100 μM)	0.88	5.0	1.23	0.38

AI-2 reporter activity was normalized to OD_{600} and culture density at the time of supernatant collection did not differ between treatments, supporting interpretation that reduced AI-2 signal reflects quorum-sensing modulation rather than decreased biomass.

Exposure of uninfected A549 cells to 100 μM mBTL did not increase LDH release relative to vehicle controls ($p > 0.05$), confirming absence of host–cell toxicity at the concentration used for infection assays.

3.4. Genotype- and AHL-Dependent Regulation of Biofilm Formation

To clarify the regulatory role of SdiA in *K. pneumoniae*, isogenic deletion mutants (ΔluxS, ΔsdiA, and ΔluxSΔsdiA) were generated in the clinical bloodstream isolate KP-PA45 and assessed for biofilm formation (A_{695}) under defined conditions with or without supplementation of 1 μM C6-HSL. Data were analyzed using two-way ANOVA (Genotype × Treatment), and model diagnostics are presented in Figure 4A–D. Under AHL-limited conditions (No AHL), deletion of sdiA resulted in a marked reduction in biofilm biomass relative to wild-type (WT: 0.480 ± 0.04; ΔsdiA: 0.205 ± 0.03). Comparable reductions were observed in ΔluxS (0.189 ± 0.03) and the double mutant (0.146 ± 0.02). The strong genotype effect is illustrated in the leverage plot (Figure 4A), and statistical testing confirmed a highly significant main effect of genotype ($F_{3,56} = 793.13$, $p < 0.0001$).

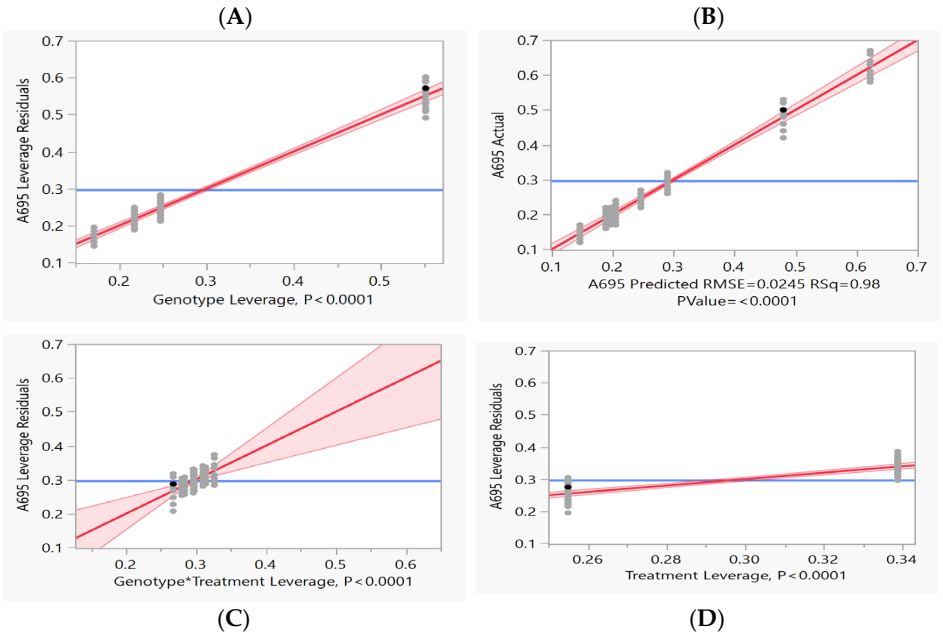


Figure 4. Two-way ANOVA analysis of genotype- and AHL-dependent regulation of biofilm formation in *K. pneumoniae* KP-PA45. (**A**) Genotype leverage plot. (**B**) Actual-by-Predicted plot. (**C**) Genotype * Treatment leverage plot. (**D**) Treatment leverage plot.

C6-HSL supplementation significantly increased WT biofilm formation (WT + C6-HSL: 0.623 ± 0.01), consistent with quorum sensing–mediated induction. The treatment leverage plot (Figure 4D) demonstrates a strong independent treatment effect ($F_{1,56}$ = 187.04, $p < 0.0001$). Critically, the Genotype × Treatment interaction was significant ($F_{3,56}$ = 11.74, $p < 0.0001$), as visualized in the interaction leverage plot (Figure 4C). This interaction indicates that the magnitude of C6-HSL responsiveness depends on the genetic background. Post hoc Tukey comparisons showed that WT + C6-HSL differed significantly from all other genotype–treatment combinations ($p < 0.001$). In contrast, ΔsdiA exhibited only modest enhancement upon C6-HSL exposure (0.290 ± 0.01), and the ΔsdiA × C6-HSL interaction term was not significant ($p = 0.9066$), indicating blunted responsiveness in the absence of SdiA. Both ΔluxS and ΔluxSΔsdiA mutants demonstrated significantly attenuated induction (interaction $p = 0.0164$ and $p = 0.0024$, respectively), suggesting coordinated LuxS–SdiA signaling is required for maximal biofilm maturation. The Actual-by-Predicted plot (Figure 4B) demonstrates excellent agreement between observed and fitted values (R^2 = 0.979; Adjusted R^2 = 0.976; RMSE = 0.0245; Model F(7,56) = 371.66, $p < 0.0001$), indicating that genotype, treatment, and their interaction collectively explain 97.9% of the variance in biofilm biomass.

3.5. Residual Distribution and Validation of Model Assumptions

To confirm the validity of ANOVA assumptions, residual diagnostics were examined (Figure 5). The residual histogram with fitted normal curve shows a symmetric distribution cantered at zero, without visible skewness or heavy tails. Quantile analysis demonstrated balanced dispersion (Q1 = −0.0163; Q3 = 0.0147), and the residual range (−0.06 to 0.05) closely matched the model RMSE (0.0245). Formal normality testing supported these observations. The Shapiro–Wilk test did not reject normality (W = 0.993, $p = 0.9738$), and the Anderson–Darling test similarly indicated no deviation from a normal distribution (A^2 = 0.171, $p = 0.9452$). Estimated parameters for the fitted normal distribution were $\mu \approx 0$ and $\sigma = 0.0231$, consistent with homoscedastic residual variance across predicted values.

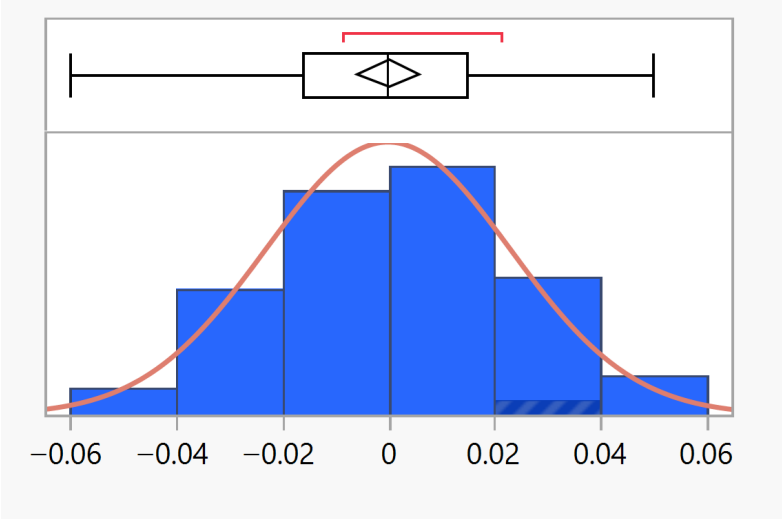


Figure 5. Residual distribution diagnostics for the two-way ANOVA model of biofilm biomass (A_{695}).

3.6. Halogenated Thiolactones Differentially Modulate LuxS and SdiA Activities

Having established that SdiA operates as a context-dependent regulator, we next examined whether a focused panel of halogenated thiolactone analogs—chloro-lactone (CL), chloro-thiolactone (CTL), meta-chloro-thiolactone (mCTL), and meta-bromo-thiolactone (mBTL)—could differentially modulate LuxS/AI-2 and SdiA signaling outputs. Although these compounds were previously reported as quorum-sensing inhibitors in *P. aeruginosa*, their activity within the hybrid LuxS–SdiA regulatory architecture of *K. pneumoniae* had not been systematically evaluated.

3.7. Effects on LuxS/AI-2 Signaling

Extracellular AI-2 accumulation was quantified using the *Vibrio harveyi* BB170 bioluminescence reporter assay following compound treatment. As summarized in Table 2, neither CL nor CTL significantly altered AI-2 levels at concentrations up to 200 µM. In contrast, mCTL and mBTL reduced AI-2 activity in a dose-dependent manner, with IC_{50} values of 8 ± 2 µM and 9 ± 2 µM, respectively. Importantly, this inhibitory effect was abolished in the ΔluxS mutant background, confirming that decreased AI-2 activity reflects interference with LuxS-dependent synthesis and/or AI-2 export rather than extracellular signal quenching or degradation.

Table 2. Differential Effects of Halogenated Thiolactones on LuxS/AI-2 and SdiA Signaling.

Compound	AI-2 Inhibition (IC_{50}, µM)	Effect in ΔluxS	Basal SdiA Activation (% of C6-HSL max)	Inhibition of C6-HSL Response (%)	Functional Classification
CL	>200 (none detected)	—	<5% (none)	<5%	Inactive
CTL	>200 (none detected)	—	<5% (none)	<5%	Inactive
mCTL	8 ± 2	Abolished	18 ± 4%	24 ± 5%	Weak partial agonist/antagonist
mBTL	9 ± 2	Abolished	32 ± 5%	41 ± 6% ($p < 0.001$)	Context-selective modulator

3.8. Effects on SdiA-Dependent Transcription

To assess direct modulation of SdiA activity, we employed *E. coli* heterologous reporter strains expressing *K. pneumoniae* SdiA and harboring a fimA–gfp transcriptional fusion. Reporter activation was quantified under basal conditions and in the presence of C6-HSL (EC_{95}). In the absence of exogenous AHL, mBTL induced weak but reproducible GFP expression (32 ± 5% of maximal C6-HSL activation), consistent with partial agonist behavior (Table S1). mCTL exhibited lower intrinsic activity (18 ± 4%), whereas CL and CTL showed negligible induction. Strikingly, when co-administered with C6-HSL at EC_{95}, mBTL reduced reporter activation by 41 ± 6% ($p < 0.001$), demonstrating competitive antagonist activity in the presence of native ligand. mCTL produced moderate inhibition (24 ± 5%), while CL and CTL again showed minimal modulation.

This ligand-dependent bidirectional behavior establishes mBTL as a context-selective SdiA modulator: it is a weak partial agonism in the absence of AHL, but a functional antagonism when competing with the native ligand. This dual pharmacology is characteristic of LuxR-type receptor modulation and likely reflects stabilization of alternative receptor conformations that permit partial DNA binding yet impair full transcriptional activation.

3.9. Transcriptomic Reprogramming

To define the global transcriptional impact of mBTL and its relationship to genetic disruption of sdiA, we performed RNA-seq on WT and ΔsdiA strains treated with vehicle or 100 μM mBTL, in the absence or presence of 1 μM C6-HSL. Multivariate structure of the dataset was first examined by principal component analysis (PCA).

Across conditions, PCA demonstrated strong separation by genotype, treatment, and AHL status. In representative correlation-based PCA plots (Figure 6A–C), Component 1 explained between 88.0% and 98.3% of the total variance, depending on condition. Under WT + mBTL + C6-HSL conditions, PC1 accounted for 98.3% of the variance, indicating highly structured transcriptional reprogramming. In contrast, ΔsdiA under No AHL conditions showed 90.4% variance explained by PC1 ($p = 0.405$), reflecting genotype-driven but more heterogeneous transcriptional dispersion. Together, these analyses confirm that both genetic disruption and chemical modulation produce coherent, condition-dependent transcriptional states.

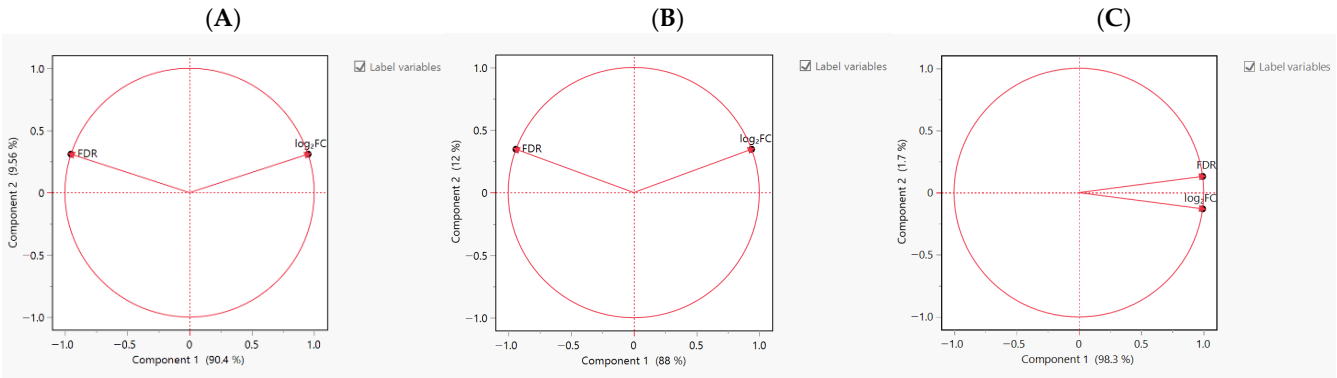


Figure 6. Transcriptomic impact of mBTL reveals signal-dependent modulation of SdiA activity. (**A**–**C**) Principal component analysis (PCA) of RNA-seq datasets under representative genotype and treatment conditions.

3.10. mBTL Phenocopies ΔsdiA Under AHL-Limited Conditions

In the absence of exogenous AHL, transcriptional changes induced by mBTL in WT cells substantially overlapped with those observed in untreated ΔsdiA. Of 342 genes differentially expressed in ΔsdiA versus WT ($|\log_2 FC| \geq 1$, FDR < 0.05), 217 (63%) were also

significantly altered in WT + mBTL versus WT. Among these overlapping genes, 189 (87%) exhibited concordant directionality of regulation (Figure 6B), indicating substantial transcriptional overlap of sdiA loss by mBTL treatment. The overlapping gene set included multiple fimbrial operons (fimA–fimK, mrkABCDF) and capsule-associated regulators (rmpA, rmpD), reinforcing the central role of SdiA in regulating surface-associated virulence determinants. This transcriptional convergence supports the interpretation that, under AHL-limited conditions, mBTL functionally mimics genetic inactivation of SdiA.

3.11. mBTL Reverses SdiA-Dependent Regulation in the Presence of AHL

Strikingly, this relationship inverted in the presence of C6-HSL. Under AHL-supplemented conditions, mBTL treatment opposed the ΔsdiA transcriptional signature (Figure 6C). Genes upregulated in ΔsdiA (representing SdiA-repressed targets) were downregulated by mBTL, whereas genes downregulated in ΔsdiA (SdiA-activated targets) were upregulated upon mBTL exposure. This bidirectional inversion is precisely the pattern expected of a competitive antagonist displacing native ligand from a LuxR-type receptor. Correlation vector plots derived from PCA further illustrate this shift. Under No AHL conditions, the loading vectors for $\log_2$FC and FDR align in a manner consistent with phenocopying of ΔsdiA. Under C6-HSL supplementation, the orientation of these vectors shifts, reflecting an opposing transcriptional trajectory consistent with antagonism.

3.12. Hierarchical Clustering Reveals Context-Dependent Network Rewiring

Hierarchical clustering of a curated panel of QS-regulated virulence genes reinforced these findings. In the absence of AHL, WT + mBTL clustered closely with ΔsdiA, distinct from untreated WT, indicating functional convergence. In contrast, under C6-HSL supplementation, WT + mBTL formed a separate cluster from both untreated WT and ΔsdiA, consistent with antagonist activity against ligand-bound SdiA. Although a contingency analysis was performed to evaluate enrichment of overlapping differentially expressed genes, the limited gene subset analyzed here resulted in insufficient cell counts for robust inference (average cell count < 5; Fisher's exact $p = 1.000$). These results highlight the necessity of performing enrichment statistics using the full transcriptome gene set rather than illustrative subsets to obtain reliable overlap significance estimates.

3.13. Mechanistic Interpretation

Collectively, these transcriptomic data demonstrate that mBTL does not function as a simple inhibitor of SdiA. Instead, its activity is signal-dependent. Under AHL-limited conditions—where SdiA predominantly exists in an apo conformation—mBTL acts as a weak partial agonist, occupying the ligand-binding pocket and inducing a receptor state that partially recapitulates sdiA loss. Conversely, under AHL-replete conditions, mBTL competes with native ligand, suppressing SdiA-dependent transcription and reversing ligand-driven gene expression programs.

3.14. Signal-Dependent Modulation of SdiA Activity

To delineate the global transcriptional consequences of mBTL exposure and its interaction with SdiA signaling, RNA-seq datasets were analyzed using principal component analysis (PCA) under representative genotype, treatment, and AHL conditions. PCA was performed on correlation matrices with row-wise variance estimation to identify dominant axes of transcriptional variance. In Table 3, the first principal component (PC1) accounted for between 88.0% and 98.3% of total variance across the analyzed conditions, indicating highly structured and condition-dependent transcriptional states. In WT cells treated with mBTL under C6-HSL supplementation, PC1 explained 98.3% of variance, demonstrating a strongly coordinated transcriptional response. In contrast, ΔsdiA under AHL-limited con-

ditions exhibited 90.4% variance explained by PC1 (p = 0.4054), reflecting genotype-driven transcriptional shifts with greater dispersion. WT treated with mBTL in the absence of AHL displayed 88.0% variance explained by PC1 (p = 0.4631), consistent with a structured but less tightly constrained transcriptional program.

Table 3. Principal Component Analysis by Condition.

Genotype	AHL	Treatment	PC1 Eigenvalue	Variance Explained (%)	PC2 Variance (%)	PC1 Significance (p-Value)
ΔsdiA	No_AHL	Vehicle	1.8088	90.44	9.56	0.4054
WT	No_AHL	mBTL	1.7604	88.02	11.98	0.4631
WT	C6_HSL	mBTL	1.9660	98.30	1.70	0.0008

Interpretation of PCA loading structure across conditions is provided in Table 4. Under No AHL conditions, WT + mBTL exhibited a transcriptional architecture consistent with phenocopying of ΔsdiA, supporting partial functional overlap between chemical modulation and genetic disruption of SdiA. However, under C6-HSL supplementation, WT + mBTL displayed a distinct transcriptional configuration characterized by near-complete variance capture by PC1, consistent with coordinated antagonism of ligand-bound SdiA activity.

Table 4. PCA Loading Interpretation Across Conditions.

Condition	PC1 Dominant Structure	Transcriptional Interpretation
ΔsdiA, No AHL	Genotype-driven	Baseline SdiA-dependent reprogramming
WT + mBTL, No AHL	Treatment-driven	Phenocopy of ΔsdiA state (partial agonism)
WT + mBTL, +C6-HSL	Ligand-structured	Antagonism of ligand-bound SdiA

4. Discussion

The development of anti-virulence strategies targeting bacterial QS remains an attractive therapeutic paradigm, yet successful implementation depends on precise understanding of target network architecture rather than simplistic receptor inhibition models [5,16]. The present study demonstrates that SdiA—the orphan LuxR-type receptor of *K. pneumoniae* —functions not as a binary virulence switch, but as a context-dependent signal integrator whose regulatory output is gated by exogenous AHL availability [13,15]. This conditional behavior reconciles previously conflicting reports in the literature and carries important implications for pharmacological targeting. Importantly, the halogenated thiolactone mBTL does not behave as a conventional "QS inhibitor" in *K. pneumoniae*. Instead, it acts as a signal-contingent modulator, with functional outcomes determined by genetic background and environmental ligand context [31]. Prior studies describing SdiA as either a positive or negative regulator of biofilm formation have produced apparently contradictory conclusions [13,32,33]. Our systematic manipulation of AHL availability provides a unifying explanation: SdiA exerts distinct regulatory outputs depending on signal context. Under AHL-limited conditions, SdiA promotes baseline biofilm development, fimbrial gene expression, and early surface attachment. In contrast, when exogenous AHLs are present—mimicking polymicrobial environments—SdiA restrains excessive biofilm maturation and modulates virulence gene expression. Thus, SdiA's regulatory polarity is environmentally gated rather than intrinsically fixed.

This model aligns with SdiA's ecological function as an inter-species signal sensor. As an orphan LuxR-type receptor lacking a cognate LuxI synthase, SdiA enables *K. pneumoniae* to detect AHL-producing neighbors. In polymicrobial niches such as the gastrointestinal

tract, urinary tract, or respiratory tract, this capacity likely allows adaptive modulation of surface-associated behaviors in response to community composition. Promoting biofilm formation in isolation but tempering it in the presence of competitors may represent an ecological optimization strategy balancing colonization and resource competition. Evidence from related Enterobacteriaceae supports this framework. In *Salmonella enterica* and *Escherichia coli*, SdiA-mediated transcription varies with AHL identity and concentration, producing distinct regulatory states. Similarly, recent work in *K. pneumoniae* indicates that C6-HSL can enhance biofilm formation while modulating virulence outputs in host models. Together, these findings reinforce the concept that SdiA operates as a conditional regulator rather than a constitutive activator or repressor.

Our data demonstrate that mBTL does not uniformly suppress SdiA activity. Instead, its pharmacological behavior mirrors the receptor's conditional biology. In the absence of native AHL, mBTL functions as a weak partial agonist, occupying the SdiA ligand-binding pocket and stabilizing a receptor conformation that supports partial transcriptional activity. In this apo context, mBTL phenocopies aspects of sdiA deletion at the transcriptional and phenotypic levels. When native AHL is present, however, mBTL competes for binding and attenuates ligand-induced activation, behaving as a competitive antagonist. This dual activity—partial agonism in the absence of ligand and antagonism in its presence—is characteristic of LuxR-family modulation and reflects stabilization of alternative receptor conformational states. Crucially, this means that the net biological effect of mBTL depends on the surrounding signal environment. Under AHL-limited conditions, mBTL attenuates biofilm formation and virulence-associated phenotypes. Under AHL-replete conditions, it may oppose SdiA-mediated repression and potentially enhance certain outputs. Thus, mBTL should be classified as a context-selective quorum-sensing modulator, not a simple inhibitor.

Although SdiA appears to be the primary functional target of mBTL in *K. pneumoniae*, our data also indicate secondary effects on the LuxS/AI-2 pathway. mBTL reduced extracellular AI-2 accumulation in a dose-dependent manner, and ΔluxS mutants exhibited altered responsiveness to mBTL in biofilm assays. This may reflect direct enzymatic inhibition of LuxS, interference with AI-2 export or uptake, or indirect regulatory cross-talk between SdiA and AI-2 signaling. Emerging evidence suggests that the LuxS and SdiA systems are not fully independent; transcriptional cross-regulation between these pathways has been described in *K. pneumoniae*. Thus, pharmacological perturbation of SdiA may propagate through the broader QS network. Further mechanistic studies will be required to determine whether mBTL directly inhibits LuxS enzymatic activity or modulates AI-2 levels via transcriptional regulation of luxS, lsr transport genes, or associated regulators.

The conditional nature of SdiA regulation presents both challenges and opportunities for anti-virulence development. The drug efficacy may vary across infection sites with differing AHL environments, the polymicrobial contexts may unpredictably alter pharmacodynamic outcomes, and the standard *in vitro* screening under AHL-free conditions may not predict in vivo performance. However, context-selective modulation may allow targeted attenuation during specific infection stages, partial agonist/antagonist profiles may preserve ecological balance in commensal populations, and precision modulation of QS networks may reduce selective pressure for resistance relative to bactericidal therapies. Rather than aiming for complete inhibition of QS receptors, future drug development efforts may benefit from designing ligands that reprogram regulatory output toward anti-virulence states irrespective of signal environment.

5. Limitations and Future Directions

Several limitations warrant consideration. First, experiments were conducted in a single clinical isolate; strain-dependent variation in QS circuitry may influence generalizability. Second, AHL supplementation was evaluated at a single concentration (1 μM); full dose–response characterization across physiological gradients is needed. Third, while infection models provide biological relevance, they do not fully recapitulate polymicrobial communities where SdiA likely exerts its natural function. Future studies should incorporate co-culture systems with defined AHL-producing species, explore structural determinants of ligand bias at SdiA, and investigate in vivo pharmacodynamics in polymicrobial infection models.

6. Conclusions

This study redefines SdiA in *K. pneumoniae* as a conditional quorum-sensing integrator whose regulatory polarity depends on the environmental ligand context. The halogenated thiolactone mBTL functions not as a uniform inhibitor but as a context-selective modulator capable of shifting SdiA-dependent transcriptional programs in opposite directions depending on signal availability. These findings underscore the necessity of understanding quorum-sensing network topology and environmental context when developing anti-virulence therapeutics and highlight ligand bias as an emerging concept in bacterial receptor pharmacology.

Supplementary Materials: The following supporting information can be downloaded at: https://www.mdpi.com/article/10.3390/applmicrobiol6040049/s1, Table S1: Differential expression status of selected SdiA-linked virulence/biofilm-associated genes (fimA, mrkA, and rmpA) across genotype (WT vs ΔsdiA), treatment (vehicle vs mBTL), and signal environment (No AHL vs C6-HSL), reporting log2 fold change, *p*-values, and differential expression classification (DE/Not_DE).

Author Contributions: Conceptualization, S.H.Y. and U.U.N.; methodology, S.H.Y.; software, S.H.Y.; validation, S.H.Y. and U.U.N.; formal analysis, S.H.Y.; investigation, S.H.Y.; resources, U.U.N.; data curation, S.H.Y.; writing—original draft preparation, S.H.Y.; writing—review and editing, S.H.Y. and U.U.N.; visualization, S.H.Y.; supervision, U.U.N.; project administration, U.U.N.; funding acquisition, U.U.N. All authors have read and agreed to the published version of the manuscript.

Funding: This research was funded by Department of Science and Innovation and the Technology Innovation Agency.

Institutional Review Board Statement: Ethical review and approval were waived for this study as it did not involve human participants or vertebrate animals. Experiments involving Galleria mellonella larvae are not subject to institutional animal ethics committee approval under South African guidelines.

Informed Consent Statement: Not applicable.

Data Availability Statement: The datasets generated and analyzed during the current study are available from the corresponding author upon reasonable request.

Acknowledgments: This work was supported by the Industrial Biocatalysis Hub.

Conflicts of Interest: The authors declare no conflicts of interest.

References

1. Abbas, R.; Chakkour, M.; Zein El Dine, H.; Obaseki, E.F.; Obeid, S.T.; Jezzini, A.; Ghssein, G.; Ezzeddine, Z. General Overview of Klebsiella pneumonia: Epidemiology and the Role of Siderophores in Its Pathogenicity. *Biology* **2024**, *13*, 78. [CrossRef]
2. Yakobi, S.H.; Nwodo, U.U. Prevalence of Antimicrobial Resistance in Klebsiella pneumoniae in the South African Populations: A Systematic Review and Meta-Analysis of Surveillance Studies. *MicrobiologyOpen* **2025**, *14*, e70037. [CrossRef]

3. Wang, M.; Wang, H. Carbapenem-resistant hypervirulent Klebsiella pneumoniae: Where is it headed in the tug-of-war between virulence and resistance? *eBioMedicine* **2025**, *114*, 105649. [CrossRef]
4. Guerra, M.E.S.; Destro, G.; Vieira, B.; Lima, A.S.; Ferraz, L.F.C.; Hakansson, A.P.; Darrieux, M.; Converso, T.R. Klebsiella pneumoniae Biofilms and Their Role in Disease Pathogenesis. *Front. Cell. Infect. Microbiol.* **2022**, *12*, 877995. [CrossRef] [PubMed]
5. Yakobi, S.H.; Ramaloko, W.; Maningi, N.E. Molecular characterization and inhibition of cyclic-di-GMP receptor proteins in Pseudomonas aeruginosa: INSIGHTS from docking and dynamics studies. *Biochem. Biophys. Rep.* **2025**, *43*, 102124. [CrossRef] [PubMed]
6. Li, Y.; Ni, M. Regulation of biofilm formation in Klebsiella pneumoniae. *Front. Microbiol.* **2023**, *14*, 1238482. [CrossRef] [PubMed]
7. Wang, Y.; Liu, B.; Grenier, D.; Yi, L. Regulatory Mechanisms of the LuxS/AI-2 System and Bacterial Resistance. *Antimicrob. Agents Chemother.* **2019**, *63*, e01186-19. [CrossRef]
8. Chen, Y.; Fan, X.; Zhu, X.; Xiao, J.; Mu, Y.; Wang, W.; Wang, C.; Peng, M.; Zhou, M. Effects of *luxS* gene on biofilm formation and fermentation property in *Lactobacillus plantarum* R. *Food Res. Int.* **2025**, *203*, 115862. [CrossRef]
9. Kanthenga, H.T.; Banicod, R.J.S.; Ntege, W.; Njiru, M.N.; Javaid, A.; Tabassum, N.; Kim, Y.-M.; Khan, F. Functional diversity of AI-2/LuxS system in lactic acid bacteria: Impacts on biofilm formation and environmental resilience. *Res. Microbiol.* **2025**, *176*, 104296. [CrossRef]
10. Zhang, Y.; Gu, Y.; Zheng, Y.; Wang, Y.; Nie, L.; Qiao, R.; He, Y. Deletion of *luxS* gene mediated by λRed gene recombination technology reduces biofilm formation and stress resistance of *Lactobacillus fermentum*. *Food Biosci.* **2022**, *49*, 101892. [CrossRef]
11. Chigozie, V.U.; Saki, M.; Esimone, C.O. Molecular structural arrangement in quorum sensing and bacterial metabolic production. *World J. Microbiol. Biotechnol.* **2025**, *41*, 71. [CrossRef] [PubMed]
12. Dai, W.; Qiao, X.; Fang, Y.; Guo, R.; Bai, P.; Liu, S.; Li, T.; Jiang, Y.; Wei, S.; Na, Z.; et al. Epigenetics-targeted drugs: Current paradigms and future challenges. *Sig. Transduct. Target Ther.* **2024**, *9*, 332. [CrossRef] [PubMed]
13. Pacheco, T.; Gomes, A.É.I.; Siqueira, N.M.G.; Assoni, L.; Darrieux, M.; Venter, H.; Ferraz, L.F.C. SdiA, a Quorum-Sensing Regulator, Suppresses Fimbriae Expression, Biofilm Formation, and Quorum-Sensing Signaling Molecules Production in Klebsiella pneumoniae. *Front. Microbiol.* **2021**, *12*, 597735. [CrossRef] [PubMed]
14. Patel, K.; Panchal, R.; Sakariya, B.; Gevariya, M.; Raiyani, R.; Soni, R.; Goswami, D. Combatting antibiotic resistance by exploring the promise of Quorum Quenching in targeting bacterial virulence. *Microbe* **2025**, *6*, 100224. [CrossRef]
15. Silva-Bea, S.; Maseda, P.; Otero, A.; Romero, M. Regulatory effects on virulence and phage susceptibility revealed by sdiA mutation in Klebsiella pneumoniae. *Front. Cell. Infect. Microbiol.* **2025**, *15*, 1562402. [CrossRef]
16. Yakobi, S.H.; Ramaloko, W.T.; Adeleke, M.A.; Pooe, O.J.; Moloantoa, K.M.; Maningi, N.E. Network-guided functional enrichment and interface-focused prioritization of quorum sensing targets in *Pseudomonas aeruginosa* for anti-virulence drug discovery. *In Silico Res. Biomed.* **2026**, *2*, 100189. [CrossRef]
17. O'Loughlin, C.T.; Miller, L.C.; Siryaporn, A.; Drescher, K.; Semmelhack, M.F.; Bassler, B.L. A quorum-sensing inhibitor blocks Pseudomonas aeruginosa virulence and biofilm formation. *Proc. Natl. Acad. Sci. USA* **2013**, *110*, 17981–17986. [CrossRef]
18. Reuter, K.; Steinbach, A.; Helms, V. Interfering with Bacterial Quorum Sensing. *Perspect. Med. Chem.* **2016**, *8*, PMC.S13209. [CrossRef]
19. Alfaraj, R.; Eltayb, E.K.; AlFayez, B.M.; Abohamad, A.; Eltahir, E.; Alenazi, N.A.; Hababah, S.; Alkahtani, H.; Almangour, T.A.; Alqahtani, F.Y.; et al. Studying the Anti-Virulence Activity of Meta-Bromo-Thiolactone against Staphylococcus aureus and MRSA Phenotypes. *Microbiol. Res.* **2023**, *14*, 1596–1609. [CrossRef]
20. Katashkina, J.I.; Hara, Y.; Golubeva, L.I.; Andreeva, I.G.; Kuvaeva, T.M.; Mashko, S.V. Use of the λ Red-recombineering method for genetic engineering of Pantoea ananatis. *BMC Mol. Biol.* **2009**, *10*, 34. [CrossRef]
21. Vilchez, R.; Lemme, A.; Thiel, V.; Schulz, S.; Sztajer, H.; Wagner-Döbler, I. Analysing traces of autoinducer-2 requires standardization of the Vibrio harveyi bioassay. *Anal. Bioanal. Chem.* **2007**, *387*, 489–496. [CrossRef]
22. Turovskiy, Y.; Chikindas, M.L. Autoinducer-2 bioassay is a qualitative, not quantitative method influenced by glucose. *J. Microbiol. Methods* **2006**, *66*, 497–503. [CrossRef] [PubMed]
23. Summer, K.; Browne, J.; Hollanders, M.; Benkendorff, K. Out of control: The need for standardised solvent approaches and data reporting in antibiofilm assays incorporating dimethyl-sulfoxide (DMSO). *Biofilm* **2022**, *4*, 100081. [CrossRef] [PubMed]
24. Born, J.; Pfeifer, F. Improved GFP Variants to Study Gene Expression in Haloarchaea. *Front. Microbiol.* **2019**, *10*, 1200. [CrossRef]
25. Chun, A.L.M.; Mosayyebi, A.; Butt, A.; Carugo, D.; Salta, M. Early biofilm and streamer formation is mediated by wall shear stress and surface wettability: A multifactorial microfluidic study. *Microbiologyopen* **2022**, *11*, e1310. [CrossRef] [PubMed]
26. Dey, S.; Gaur, M.; Sykes, E.M.E.; Prusty, M.; Elangovan, S.; Dixit, S.; Pati, S.; Kumar, A.; Subudhi, E. Unravelling the Evolutionary Dynamics of High-Risk Klebsiella pneumoniae ST147 Clones: Insights from Comparative Pangenome Analysis. *Genes* **2023**, *14*, 1037. [CrossRef]
27. Stupnikov, A.; McInerney, C.E.; Savage, K.I.; McIntosh, S.A.; Emmert-Streib, F.; Kennedy, R.; Salto-Tellez, M.; Prise, K.M.; McArt, D.G. Robustness of differential gene expression analysis of RNA-seq. *Comput. Struct. Biotechnol. J.* **2021**, *19*, 3470–3481. [CrossRef]

28. O'Toole, G.A. Microtiter Dish Biofilm Formation Assay. *J. Vis. Exp.* **2011**, 2437. [CrossRef]
29. Ménard, G.; Rouillon, A.; Cattoir, V.; Donnio, P.-Y. Galleria mellonella as a Suitable Model of Bacterial Infection: Past, Present and Future. *Front. Cell. Infect. Microbiol.* **2021**, *11*, 782733. [CrossRef]
30. Peivandi, Z.; Shirazi, F.H.; Teimourian, S.; Farnam, G.; Babaei, V.; Mehrparvar, N.; Koohsari, N.; Ashtarinezhad, A. Silica nanoparticles-induced cytotoxicity and genotoxicity in A549 cell lines. *Sci. Rep.* **2024**, *14*, 14484. [CrossRef]
31. Wang, L.; Zhang, Y.; Liu, Y.; Xu, M.; Yao, Z.; Zhang, X.; Sun, Y.; Zhou, T.; Shen, M. Effects of chlorogenic acid on antimicrobial, antivirulence, and anti-quorum sensing of carbapenem-resistant Klebsiella pneumoniae. *Front. Microbiol.* **2022**, *13*, 997310. [CrossRef]
32. Culler, H.F.; Couto, S.C.F.; Higa, J.S.; Ruiz, R.M.; Yang, M.J.; Bueris, V.; Franzolin, M.R.; Sircili, M.P. Role of SdiA on Biofilm Formation by Atypical Enteropathogenic Escherichia coli. *Genes* **2018**, *9*, 253. [CrossRef]
33. Hai, H.; Yang, M.; Cheng, Z.; Ma, K.; Shang, F. Potential Role of SdiA in Biofilm Formation and Drug Resistance in Avian Pathogenic Escherichia coli. *Animals* **2024**, *14*, 2199. [CrossRef]

Disclaimer/Publisher's Note: The statements, opinions and data contained in all publications are solely those of the individual author(s) and contributor(s) and not of MDPI and/or the editor(s). MDPI and/or the editor(s) disclaim responsibility for any injury to people or property resulting from any ideas, methods, instructions or products referred to in the content.